Dripping faucet dynamics is determined by synchronization of drop oscillations and detachment

Ariel Shemesh,[1,*] Solange Akselrod,[1,†] Ziv Reich,[2] Dan Shahar,[3] and Ruti Kapon[2,‡]
[1]*Abramson Center for Medical Physics, Department of Physics and Astronomy, Tel Aviv University, Tel Aviv 69978, Israel*
[2]*Department of Biological Chemistry, Weizmann Institute of Science, Rehovot 76100, Israel*
[3]*Department of Condensed-Matter Physics, Weizmann Institute of Science, Rehovot 76100, Israel*
(Received 13 February 2012; published 21 August 2012)

A dripping faucet is an example of an everyday system that exhibits surprisingly rich dynamics ranging from periodic to chaotic. Using a simple capacitive device, we experimentally demonstrate that the dynamics is determined by the degree of synchronization between two temporally disparate processes: the time at which a drop attains a critical mass and an oscillatory process that accompanies the formation of a drop. We present a full experimental phase-space reconstruction of the ensuing dynamics.

DOI: 10.1103/PhysRevE.86.026209 PACS number(s): 05.45.−a, 47.55.D−, 47.52.+j, 84.37.+q

A dripping faucet exhibits surprisingly rich dynamics that arises from an intricate interplay between the time scales involved in the dripping process. These time scales can be very different from each other because of their dependence on the physical parameters that influence the flow [1–3]: the surface tension and the viscosity of the fluid, and the external forces acting on the drops. Since its introduction by Shaw and coworkers as a paradigm for everyday chaotic behavior [4,5], the dripping faucet has been the subject of extensive experimental and theoretical investigations [2,3,6–14]. A common practice among the researchers in this field has been to divide the treatment of the dripping process into two distinct regimes. The first is the formation of individual drops, governed largely by the interplay between hydrodynamics and surface tension, including the strong nonlinearities that develop in conjuncture with the drop breakup [1,15–21]. The second regime deals with the time evolution of dripping of the formed drops, with its very rich dynamics, culminating with the emergence of chaotic behavior [3,6–14].

This artificial division occurs not only because the theoretical tools and frameworks needed in order to understand these processes are different but also because their measurement requires distinct techniques: The formation of drops has conventionally been studied using high-speed and high-resolution video capturing necessary to pinpoint the liquid-surface breaking event [15–21], while for the dripping dynamics, whose study requires acquisition of long, discrete time traces $\{T(n)\}$, a laser-based drop-counter apparatus is typically employed [5–9,11,12,22]. In these latter measurements, information regarding drop development cannot be recorded. This division obscures a central aspect of the dripping process that was recently discovered by several theoretical groups [2,13,14], namely the significance of synchronization, between different processes that occur during dripping on the dynamics.

To circumvent this difficulty, we developed a simple device comprising an electrical capacitor near the nozzle of a pipette, which allows monitoring of the dripping process at high temporal resolution over a long time, giving us access to all relevant time scales. This enabled us to concomitantly study both drop formation and dripping. Our method employs custom-made nozzles that incorporate two facing electrodes, whose mutual capacitance during the dripping process reflects the development of drops emanating from the nozzle (Figs. 1 and 2). The capacitance signal is continuous, simple to measure, and correlates with the various stages of drop formation from buildup to breakup (Fig. 2).

Two types of nozzles were constructed: pipettes made of either glass or quartz, on which electrodes were placed to form the capacitor. The glass nozzles served for the measurements of the dynamics and were made from commercial Pasteur pipettes that had an inner diameter of 6.9 mm and outer diameter of 8.96 mm. Two conductive adhesive strips, which were placed along the pipettes facing each other, served as the capacitor. Smaller quartz nozzles, which had an inner diameter of 0.5 mm and an outer diameter of 1 mm, were used to establish the correlation between the capacitance signal and dripping. For these nozzles, the two facing electrodes were made of evaporated Ti-Au strips. In all experiments, capacitance between the electrodes was monitored by measuring the voltage across the balancing arm of a ratio-arm transformer capacitance bridge, using a standard ac lock-in technique employing an excitation voltage of 5 V at 10 KHz. The fluid we used was double-distilled water with a resistance of $\geqslant 17$ MΩ. To drive the liquid through the glass pipette, we used a gravitational-based system that maintains a fixed water level (Fig. 1). For the small quartz pipette, a syringe pump drove the flow at a desired constant rate with $\pm 2\%$ accuracy.

All experiments were conducted in an enclosed chamber, at $22\,^{\circ}\mathrm{C} \pm 0.5\,^{\circ}\mathrm{C}$, which provided both electrical and mechanical noise isolation. The entire setup was mounted on an optical table to prevent vibrations.

Figure 2 demonstrates the correlation between the capacitance signal, acquired at a rate of 5000 Hz, and the evolution of a single drop recorded by time-lapse video images of the forming drops at a rate of 44 frames per second. The solid line in Fig. 2 shows the capacitance trace measured during the buildup of one drop in the small quartz nozzle. To exemplify the geometry of the drop at the various stages of drop formation, we superimposed on the trace, at the appropriate time points, microscope images of the drops. As can be seen,

*Present address: Schulich Faculty of Chemistry, Technion—Israel Institute of Technology, Haifa 32000, Israel.
†Deceased.
‡Author to whom correspondence should be addressed: ruti.kapon@weizmann.ac.il

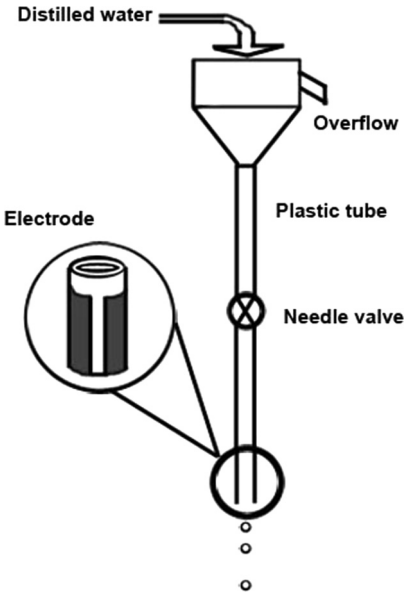

FIG. 1. The measurement system: The water dispenser applies constant pressure to the needle valve connected to the nozzle. Closeup: Glass nozzle with two conducting electrodes facing each other, forming a capacitor. This capacitor allows measurement of variations in drop geometry during formation and breakup. For the measurements on the small nozzle a syringe pump replaced the water dispenser.

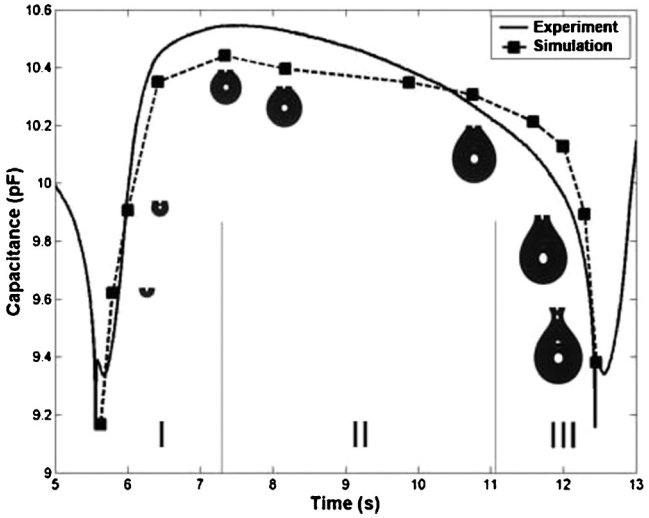

FIG. 2. Capacitance measurement of the buildup of a single drop: Experimental (solid line) and simulation (full square) results together with the images of the drop that was used for the simulation calculation. Water flowed at a rate of 20 ml/h giving rise to dripping at 0.133 drops through the smaller quartz pipette. Images were recorded using a JAI CV-M4 + CL digital camera synchronized to the capacitance measurements through a house-written LABVIEW program. Regions I, II and III depict three different stages in drop evolution. The dashed line is used to guide the eye.

the evolution and breakup of a drop has a clear signature in the capacitance trace.

The capacitance between the two electrodes depends on the dielectric properties of the materials that surround the capacitor and the geometry that they occupy in space. Since the highest electric field is at the edge of the electrodes, the part of the drop that is closest to the nozzle has the largest effect on the capacitance. It is thus not only the volume of the drop but also the thickness of the water bridge near the nozzle that influences the capacitance.

To further illustrate the relation between the formation of the drop and the capacitance trace we calculated the capacitance by solving the three-dimensional Poisson equation for a geometry obtained from the video images, considering axially symmetric drops. The results of this calculation are plotted as solid squares in Fig. 2. A clear correspondence between the measured capacitance and the calculated capacitance is evident. The capacitance signal acquired, therefore, provides a high-fidelity representation of the drop formation process.

To obtain time series from our capacitance traces, we first identified a single dripping event and then calculated the cross-correlation of this event with the time trace obtained during the entire flow. The dripping events are then identified with the instances of time for which the cross-correlation function has a maximum and the time intervals are the time differences between adjacent maxima.

Figures 3(a)–3(c) show capacitance measurements, obtained for average drip rates of 1.8, 2, and 3.25 drops per second (drops/s) from a glass tube with an internal diameter of 6.9 mm. Each period in the traces corresponds to the evolution of a single drop and consists of a component describing the overall growth and detachment of the drop, on which an oscillatory signal is superimposed. During the first stage [region I in Fig. 2 and Fig. 3(a)], the drop grows, due to the flow of water into it, while surface tension maintains its spherical shape. At this stage, the capacitance increases because the volume of liquid near the capacitor increases. As water continues to flow into the drop, gravity force begins to overcome the surface tension and the drop develops into a pear shape with a narrow neck. This necking lowers the volume of liquid near the nozzle and leads to a reduction in capacitance. At first, neck formation is slow and only a mild decrease in capacitance appears [region II in Fig. 2 and Fig. 3(a)]. As the drop approaches its critical volume the neck diameter decreases rapidly, resulting in a sharp decrease in capacitance until the drop breaks up [region III Fig. 2 and Fig. 3(a)]. At this point the capacitance signal reaches its minimum value.

An interesting feature seen in the time traces at all dripping rates is the appearance of oscillations in the capacitance signal. These oscillations are a manifestation of the interplay between the force due to gravity, which pulls the drop down, and surface tension, which pulls it up [5,12,13,17,23–27]. The oscillations of the drop affect the time period between successive drops and are central to the determination of the dynamics of the system [6,13,26,27]. For a flow rate of 1.8 drops/s [Fig. 3(a)] seven oscillations occur during the slow buildup stage of the drop [area II in Fig. 3(a)]. An eighth oscillation sometimes emerges at slightly different points in the rapid necking stage. The structure of the capacitance trace for each drop is thus slightly different. The dripping dynamics can be conveniently studied by constructing a time return map consisting of a plot of the time interval between consecutive drops $T(n)$, as a function of the time interval between the previous pair of consecutive drops $T(n-1)$. The return map for dripping at 1.8 drops/s

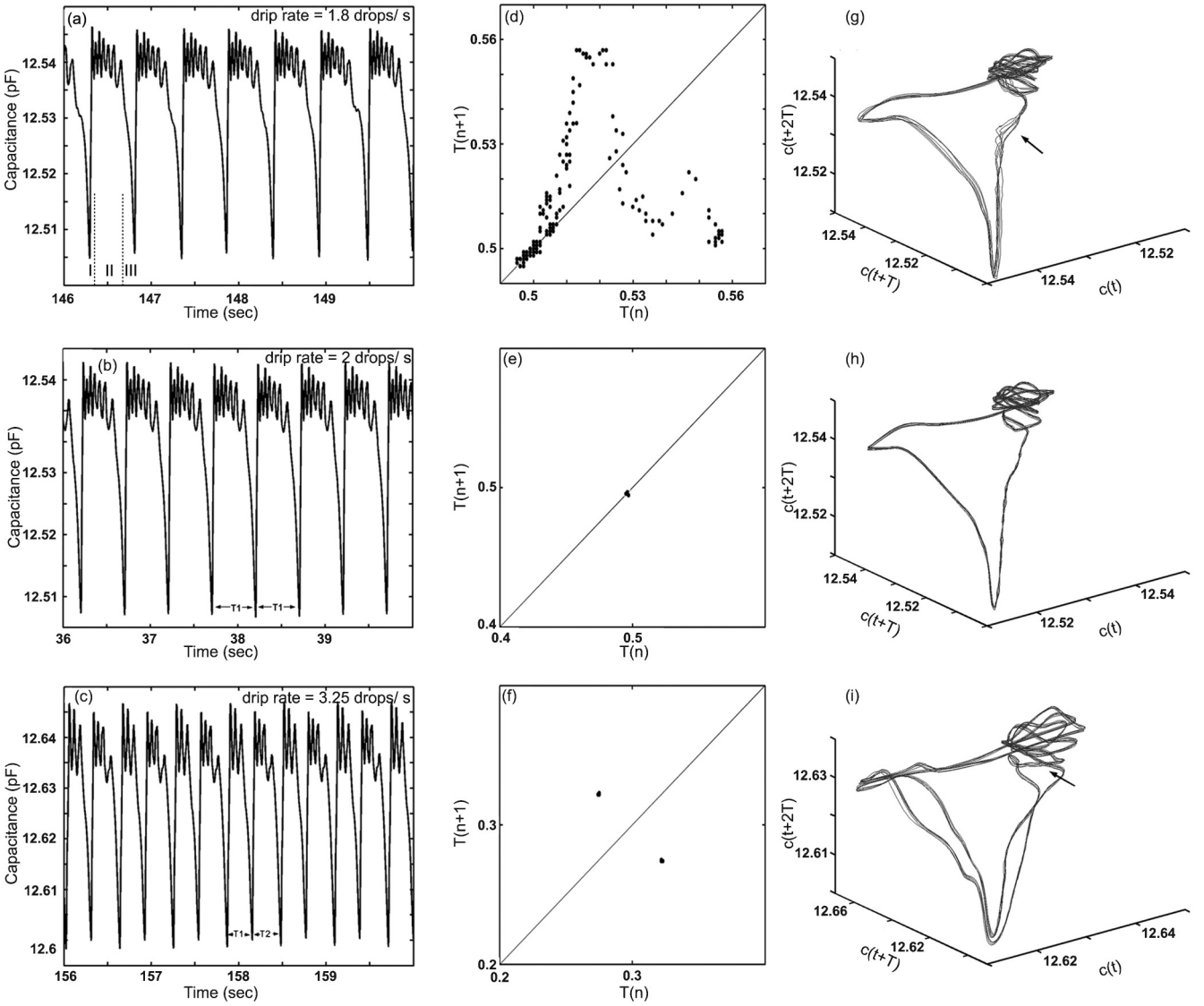

FIG. 3. Capacitance trace, time return maps, and phase space of dripping. (a)–(c) Dripping traces for chaotic (at an average drip rate of 1.8 drops/s), periodic (at an average drip rate of 2 drops/s), and period-two dynamics (at an average drop rate of 3.25 drops/s), respectively. (d)–(f) Time return maps constructed from the dripping traces. (g)–(i) Phase space corresponding to the dripping trace. In (g) and (i) the arrow points to the last oscillation.

is shown in Fig. 3(d) and indicates that the dripping at this flow rate is chaotic and is characterized by a single strange attractor. For a slightly higher drip rate of 2 drops/s, the eighth oscillation cannot develop and oscillations are synchronized with the time it takes a drop to reach its critical mass leading to a single period of dripping. Looking at the dripping time trace one sees that all drops exhibit nearly identical capacitance traces, comprised of seven oscillations and having a similar magnitude dip in the capacitance. Periodic behavior is evident in the return map as a single point on the diagonal of the graph [Fig. 3(e)]. At an average drip rate of 3.25 drops/s, we observe two alternating patterns of the evolution of individual drops. The first pattern [T_1 in Fig. 3(c)] incorporates three oscillations, while the second [T_2 in Fig. 3(c)] has an additional, smaller amplitude oscillation. The T_2 pattern also has a larger dip of the capacitance than that of T_1, indicating that the drop broke off at a narrower neck than that of T_1. As a result of the appearance of two alternating patterns in the capacitance trace, we now obtain two points mirrored about the diagonal [Fig. 3(f)] in the return map indicating period-two dynamics.

To illustrate the effect of the oscillations on the dynamics we use a simplified model that carries the main ingredients of the actual process. In this model, the detachment of a drop occurs when the force on the neck exceeds the maximal surface tension f_s that the liquid can support. For the static case, this occurs when the drop reaches a mass m defined by the relation $mg = f_s$ (g is the acceleration due to gravity). When oscillations occur, the accelerated motion of the drop exerts an additional force on the liquid neck modifying the condition for detachment: $f_s = mg - ma$. During a downward motion this force acts in the direction of gravity reducing the mass necessary to overcome surface tension and thereby the time it takes to attain this mass. During an upward motion the force acts in the direction opposite to gravity and detachment

will occur only when the drop attains a higher mass after a longer time. In this way, oscillations modulate the time of drop detachment and the ensuing dripping dynamics.

A different way to describe a dynamical system is to reconstruct its trajectory in multidimensional phase space. This requires a continuous parameter and therefore such reconstructions have been presented in theoretical [13,27] but not in experimental studies of dripping. We used our capacitance measurement as a continuous parameter in order to reconstruct the phase space using the time delay method [28]. In this method, for a single observable x_j, d-dimensional pseudovectors y_j are built, with elements being the sampled observable separated by a constant delay time such that $y_j = [x_j; x_{j+h}; \ldots; x_{j+h(d-1)}]$, where h is the delay index, and d the embedding dimension, both of which are to be determined. We first calculated the optimal time delays using the average mutual information function and found it to be $T = 16$ ms for the period-one reconstruction, $T = 21$ ms for period-two reconstruction, and $T = 17$ ms for the chaotic reconstruction. Next, we calculated the embedding dimension and found it to be $d = 3$. For this purpose we used the false nearest neighbors (FNN) method that finds the nearest neighbor of every point in a given dimension, then checks to see if these points are still close neighbors in one higher dimension. Finally, we used the time delay method to build the three-dimensional graph in which the x, y, z axes correspond to $C(t)$, $C(t + T)$, $C(t + 2T)$, respectively [Figs. 3(g)–3(i)].

The long trajectory in all reconstructions corresponds to drop buildup and breakup, which occurs at the bottom of each cycle [27]. Oscillations are most apparent in the upper right of the reconstructions where the radius of the drop near the tip of the capillary changes slowly. They trace an irregular spiral whose radius decreases very slowly indicating that damping is not significant in our experiments. The reconstruction shows that the stage at which the last oscillation appears in each drop [marked by arrows in Figs. 3(g) and 3(i)] determines the type of dynamics that will ensue. Figure 3(g) shows the phase space for chaotic dynamics. The last oscillation, in every path (see arrow), occurs in a developed stage of instability after the saddle node bifurcation, where the neck is rapidly decreasing in radius. The time of breakup is thus extremely sensitive to the exact point at which this oscillation occurs and the resulting phase space shows many different paths for the evolution of drops and consequently, chaotic dynamics. On the other hand, for a drip rate of 2 drops/s the last oscillation occurs within the spiral, prior to the saddle node bifurcation and does not affect the onset of drop pinch-off, resulting in a single trajectory in phase space and period-one dynamics. Figure 3(i) contains two distinct trajectories where every second trajectory has an extra oscillation (see arrow) as described in the previous section. This extra oscillation occurs close to the saddle point and thus forces the drop into one of two stable solutions resulting in period-two behavior. These results recreate the theoretical phase space predicted by Coullet *et al.* [13,27] and are in good agreement with the simple interpretation we presented earlier based on the capacitance time traces.

In summary, using a capacitance-based method, we have shown that synchronization between the oscillatory processes that accompany drop formation and drop breakup leads to the rich dynamics observed in dripping faucet experiments and have provided an experimentally measured phase-space reconstruction of the dripping process.

D.S.'s research was supported by the Minerva Foundation with funding from the Federal German Ministry for Education and Research.

[1] J. Eggers, Phys. Fluids **7**, 941 (1995).
[2] N. Fuchikami, S. Ishioka, and K. Kiyono, J. Phys. Soc. Jpn. **68**, 1185 (1999).
[3] B. Ambravaneswaran, S. D. Phillips, and O. A. Basaran, Phys. Rev. Lett. **85**, 5332 (2000).
[4] R. Shaw, *The Dripping Faucet as a Model Chaotic System* (Aerial Press, Santa Cruz, CA, 1984).
[5] P. Martien, S. C. Pope, P. L. Scott, and R. S. Shaw, Phys. Lett. A **110**, 399 (1985).
[6] K. Kiyono, T. Katsuyama, T. Masunaga, and N. Fuchikami, Phys. Lett. A **320**, 47 (2003).
[7] X. Wu, E. Tekle, and Z. A. Schelly, Rev. Sci. Instrum. **60**, 3779 (1989).
[8] T. Katsuyama and K. Nagata, J. Phys. Soc. Jpn. **2**, 396 (1999).
[9] K. Dreyer and F. R. Hickey, Am. J. Phys. **59**, 619 (1991).
[10] P. M. C. de Oliveira and T. J. P. Penna, J. Stat. Phys. **73**, 789 (1993).
[11] R. D. Pinto, W. M. Goncalves, J. C. Sartorelli, and M. J. de Oliveira, Phys. Rev. E **52**, 6896 (1995).
[12] A. D'Innocenzo, F. Paladini, and L. Renna, Phys. Rev. E **65**, 056208 (2002).
[13] P. Coullet, L. Mahadevan, and C. S. Riera, J. Fluid Mech. **526**, 1 (2005).
[14] H. J. Subramani, H. K. Yeoh, R. Suryo, Q. Xu, and B. Ambravaneswaran, Phys. Fluids **18**, 032106 (2006).
[15] X. D. Shi, M. P. Brenner, and S. R. Nagel, Science **265**, 219 (1994).
[16] R. M. S. M. Schulkes, J. Fluid Mech. **278**, 83 (1994).
[17] X. Zhang and O. A. Basaran, Phys. Fluids **7**, 1184 (1995).
[18] X. Zhang, J. Colloid Interface Sci. **212**, 107 (1999).
[19] D. M. Henderson, W. G. Pritchard, and L. B. Smolka, Phys. Fluids **9**, 3188 (1997).
[20] E. D. Wilkes, S. D. Phillips, and O. A. Basaran, Phys. Fluids **11**, 3577 (1999).
[21] A. U. Chen, P. K. Notz, and O. A. Basaran, Phys. Rev. Lett. **88**, 174501 (2002).
[22] R. D. Pinto and J. C. Sartorelli, Phys. Rev. E **61**, 342 (2000).
[23] K. Kiyono and N. Fuchikami, J. Phys. Soc. Jpn. **68**, 3259 (1999).
[24] Y. Watanabe, Jpn. J. Appl. Phys. **24**, 351 (1985).
[25] M. S. F. da Rocha, J. C. Sartorelli, W. M. Goncalves, and R. D. Pinto, Phys. Rev. E **54**, 2378 (1996).
[26] A. D'Innocenzo and L. Renna, Int. J. Theor. Phys. **35**, 941 (1996).
[27] P. Coullet, L. Mahadevan, and C. Riera, Prog. Theor. Phys. Suppl. **139**, 507 (2000).
[28] F. Takens, in *Detecting Strange Attractors in Turbulence* (Springer, Berlin-Heidelberg-New York, 1981), p. 366.